Spin Polarization and Texture of the Fermi Arcs in the Weyl Fermion Semimetal TaAs

Su-Yang Xu *et al.*

Phys. Rev. Lett. **116**, 096801 — Published 1 March 2016

DOI: 10.1103/PhysRevLett.116.096801

Spin polarization and texture of the Fermi arcs in the Weyl Fermion semimetal TaAs

Su-Yang Xu*,[1] Ilya Belopolski*,[1] Daniel S. Sanchez*,[1] Madhab Neupane*,[1,2,3] Guoqing Chang,[4,5] Koichiro Yaji,[6] Zhujun Yuan,[7] Chenglong Zhang,[7] Kenta Kuroda,[6] Guang Bian,[1] Cheng Guo,[7] Hong Lu,[7] Tay-Rong Chang,[8] Nasser Alidoust,[1] Hao Zheng,[1] Chi-Cheng Lee,[4,5] Shin-Ming Huang,[4,5] Chuang-Han Hsu,[4,5] Horng-Tay Jeng,[8,9] Arun Bansil,[10] Titus Neupert,[11] Fumio Komori,[6] Takeshi Kondo,[6] Shik Shin,[6] Hsin Lin,[4,5] Shuang Jia,[7,12] and M. Zahid Hasan†[1]

[1]*Laboratory for Topological Quantum Matter and Spectroscopy (B7), Department of Physics, Princeton University, Princeton, New Jersey 08544, USA*

[2]*Condensed Matter and Magnet Science Group, Los Alamos National Laboratory, Los Alamos, NM 87545, USA*

[3]*Department of Physics, University of Central Florida, Orlando, Florida 32816, USA*

[4]*Centre for Advanced 2D Materials and Graphene Research Centre National University of Singapore, 6 Science Drive 2, Singapore 117546*

[5]*Department of Physics, National University of Singapore, 2 Science Drive 3, Singapore 117542*

[6]*The Institute for Solid State Physics (ISSP), University of Tokyo, Kashiwa, Chiba 277-8581, Japan*

[7]*International Center for Quantum Materials, School of Physics, Peking University, China*

[8]*Department of Physics, National Tsing Hua University, Hsinchu 30013, Taiwan*

[9]*Institute of Physics, Academia Sinica, Taipei 11529, Taiwan*

[10]*Department of Physics, Northeastern University, Boston, Massachusetts 02115, USA*

[11]*Joseph Henry Laboratory, Department of Physics,*

* These authors contributed equally to this work.

† Corresponding author: mzhasan@princeton.edu

Princeton University, Princeton, New Jersey 08544, USA

[12]*Collaborative Innovation Center of Quantum Matter, Beijing,100871, China*

(Dated: January 19, 2016)

Abstract

A Weyl semimetal is a new state of matter that hosts Weyl fermions as quasiparticle excitations. The Weyl fermions at zero energy correspond to points of bulk band degeneracy, Weyl nodes, which are separated in momentum space and are connected only through the crystal's boundary by an exotic Fermi arc surface state. We experimentally measure the spin polarization of the Fermi arcs in the first experimentally discovered Weyl semimetal TaAs. Our spin data, for the first time, reveal that the Fermi arcs' spin polarization magnitude is as large as 80% and lies completely in the plane of the surface. Moreover, we demonstrate that the chirality of the Weyl nodes in TaAs cannot be inferred by the spin texture of the Fermi arcs. The observed non-degenerate property of the Fermi arcs is important for establishing its exact topological nature, which reveals that spins on the arc form a novel type of 2D matter. Additionally, the nearly full spin polarization we observed ($\sim 80\%$) may be useful in spintronic applications.

The Weyl semimetal can potentially open a new era in condensed matter physics and materials science as it provides the first realization of Weyl fermions, broadens the classification of topological phases beyond insulators, demonstrates exotic quantum anomalies, and exhibits novel Fermi arc surface states [1–19]. A Weyl semimetal has a band structure with band crossings between two non-degenerate bands, Weyl nodes, which are each associated with a quantized chiral charge [7]. It can be understood as a monopole or an anti-monopole of the Berry curvature in momentum space. Remarkably, the protection of the Weyl fermions does not require any symmetry besides translation. Weyl semimetals may exhibit exceptionally high electron mobilities [14] and may be used to improve electronics by carrying electric currents more efficiently. Moreover, the presence of parallel electrical and magnetic fields can break the apparent conservation of the chiral charge due to the chiral anomaly, making a Weyl metal, unlike ordinary nonmagnetic metals, more conductive with an increasing magnetic field. Furthermore, the Weyl nodes are connected only through the crystal's boundary by a topological surface state, a Fermi arc. These phenomena make new physics accessible and suggest potential applications [21–29].

Very recently, the first Weyl semimetal has been experimentally discovered in an inversion breaking, single-crystalline compound TaAs [12, 15]. Both the Weyl fermions and the Fermi arcs have been directly observed by photoemission spectroscopy [12, 15]. Here, we study the spin polarization properties of the topological Fermi arc surface states in TaAs. Historically, the surface spin texture has played a crucial role for topological insulators because it reveals the π Berry phase that demonstrates the nontrivial topology [30–32]. A Weyl semimetal can be thought of as an interpolation between topological and normal insulators [6]. Hence, it is important to understand the topological meaning of the Fermi arcs' spin texture in a Weyl semimetal. We use our spin data and calculation of the Fermi arcs in TaAs to study this important topic.

Laser-based spin-resolved angle-resolved photoemission spectroscopy (laser-SARPES) measurements were performed at the Institute for Solid State Physics (ISSP) at the University of Tokyo. Photoelectrons were excited by an ultraviolet laser ($h\nu = 6.994$ eV). The spin polarization was detected by the very-low-energy electron diffraction (VLEED) spin detectors using pre-oxidized Fe(001)-p(1×1)-O targets. The two spin detectors were placed at an angle of 90 deg. and were directly attached to a ScientaOmicron DA30-L analyzer, enabling simultaneous spin-resolved ARPES measurements for all three spin components

as well as high-resolution spin-integrated ARPES experiments. The energy and angle resolutions were set to be better than 20 meV and 0.7° for the laser-SARPES measurements. Spin-integrated ARPES measurements were performed at beamlines 4.0.3 of the Advanced Light Source (ALS) at the Lawrence Berkeley National Laboratory (LBNL) in Berkeley, California, USA. The energy and momentum resolution of the vacuum ultraviolet ARPES instruments was better than 30 meV and 1% of the surface Brillouin zone (BZ). For all measurements, Samples were measured at a temperature of about 20 K and under a vacuum condition better than 1×10^{-10} torr. First-principles calculations were performed by using the OPENMX code based on norm-conserving pseudopotentials generated with multi-reference energies and optimized pseudoatomic basis functions within the framework of the generalized gradient approximation (GGA) of density functional theory (DFT) [33]. Spin-orbit coupling was incorporated through j-dependent pseudo-potentials. For each Ta atom, three, two, two, and one optimized radial functions were allocated for the s, p, d, and f orbitals ($s3p2d2f1$), respectively, with a cutoff radius of 7 Bohr. For each As atom, $s3p3d3f2$ was adopted with a cutoff radius of 9 Bohr. A regular mesh of 1000 Ry in real space was used for the numerical integrations and for the solution of the Poisson equation. A k point mesh of $17 \times 17 \times 5$ for the conventional unit cell was used and experimental lattice parameters [34] were adopted in the calculations. Symmetry-respecting Wannier functions for the As p and Ta d orbitals were constructed without performing the procedure for maximizing localization and a real-space tight-binding Hamiltonian was obtained [35]. The surface state band structure and spin polarization were calculated by the surface Green's function technique, which computes the spectral weight near the surface of a semi-infinite system.

Let us first discuss the essential aspects of the surface state band structure that are important for our investigation of the spin texture. TaAs crystalizes in a body-centered tetragonal lattice system with the space group of $I4_1md$ (#109). Systematic details of the band structures can be found in Ref. [12]. Figure 1(a) shows a schematic illustration of TaAs's crystal lattice. It can be seen that the lattice lacks a space-inversion center, which is key to realizing the time-reversal symmetric Weyl semimetal state [6]. First principles calculations showed 24 Weyl nodes in the bulk Brillouin zone (BZ). On the (001) surface of the TaAs, the 24 Weyl nodes project onto 16 points. Eight projected Weyl nodes near the surface BZ boundary ($\bar{X}$ and $\bar{Y}$ points) have a projected chiral charge of ± 1. The other eight projected Weyl nodes close to midpoints of the $\bar{\Gamma} - \bar{X}(\bar{Y})$ lines have a projected chiral

charge of ± 2. They are shown by black and white dots in Fig. 1(b). The calculated surface state Fermi surface is in excellent agreement with the ARPES data in Ref. [12]. Specifically, we identify three main features, namely a bowtie-shaped contour at the $\bar{Y}$ point, an elliptical contour at the $\bar{X}$ point, and a crescent-shaped feature near the midpoint of each $\bar{\Gamma} - \bar{X}(\bar{Y})$ line. Our investigation focuses on the crescent-shaped feature that consists of two curves (Fermi arcs) that join each other at the two end points, which correspond to projected Weyl nodes with projected chiral charge of ± 2. The Fermi arcs near the $\bar{X}$ and $\bar{Y}$ points were not well-resolved in ARPES due to the close proximity of the corresponding Weyl nodes [12]. Hence we only focus on the crescent Fermi arcs near the midpoint of each $\bar{\Gamma} - \bar{X}(\bar{Y})$ line.

Figure 1(c) shows the calculated spin texture of the crescent Fermi arcs. Denoted by white arrows is the direction of spin polarization along the Fermi arcs. The direction of spin polarization rotates clockwise as one travels around the outer Fermi arc in a counter-clockwise fashion. If one travels along the inner arc in an counter-clockwise fashion, we observe that the spin direction also rotates clockwise. The actual spin polarization direction for the extrema of the outer and inner Fermi arcs are opposite to each other. An observation to make here is the constraint mirror symmetry enforces on the allowed spin polarization direction. As illustrated in Fig 1c, the crescent Fermi arcs intersect the high-symmetry line $(\bar{\Gamma} - \bar{Y})$, which is invariant under the reflection $\mathcal{M}_x : x \Rightarrow -x$. This crescent Fermi arc lies on a high symmetry line that cuts along the middle of both arcs. This mirror symmetry should therefore only allow, for the case of Fig. 1(c), in-plane spin polarization direction along $\pm k_x$, which is consistent with our calculations for the spin texture at extrema of both inner and outer arcs. In Fig. 2(a) we show a high-resolution ARPES Fermi surface map of crescent Fermi arcs. Labeled on Fig. 2(a) are the k_i points ($i = 1, 2, 3, 4, 5$) on the outer Fermi arc that corresponds to the spin polarization direction calculated, shown in Fig. 2(b), and experimentally measured, shown in Figs. 2(c-g). The spin polarization direction at k_1, the extremum of the outer arc, was measured to be nearly 80% along the $+k_x$ direction and no spin polarized along the $\pm k_y$ direction within our experimental resolution, which is consistent with our calculations in Fig. 2(b). In addition, the measured spin polarization direction at k_2 and k_3 shows 40% spin polarization along $+k_x$ and $-k_y$ direction and 40% spin polarization along $+k_x$ and $+k_y$ direction, respectively. Finally, the measured spin polarization direction for the outer Fermi arc at k_4 and k_5, shows 0% spin polarization along $\pm k_x$ and 80% in the $-k_y$ direction and $+k_y$ direction, respectively. By comparing

the in-plane spin polarization direction defined in Figs. 2(c-g) with spin texture calculated and displayed in Fig. 2(b), it becomes apparent that our experimental results are consistent with our theoretical predictions.

Lets now perform a similar spin texture analysis on the inner crescent Fermi arc. In Fig. 3(a) we present the same Fermi surface map of the Fermi arcs presented in Fig. 2(a), but now the inner Fermi arc is labeled with k_i points ($i = 6, 7, 8$). A schematic illustration of the spin texture predicted by calculation is shown in Fig. 3(b), with the spin polarization direction denoted by white arrows. The spin polarization direction at k_6, the extremum of the inner arc, was measured to be nearly 80% along the $-k_x$ direction and approximately 0% spin polarized along the $\pm k_y$ direction, which is consistent with our calculations in Fig. 3(b). Now, the measured spin polarization direction at k_7 and k_8 shows 45% spin polarization along $-k_x$ and $+k_y$ direction and $30\% - 40\%$ spin polarization along $-k_x$ and $-k_y$ direction, respectively. Similar to the outer Fermi arc presented in Fig. 2, the spin texture calculated and exhibited in Fig. 2(b) is consistent with our experimental results shown in Figs. 3(c-e). Our data (Fig. 3(f)) show that the measured spin polarization is consistent with the calculated spin polarization of the Fermi arcs, irrespective of the light polarization.

The out-of-plane spin polarization data are shown in Fig. 4(a). From the data, it is clear that no out-of-plane spin (P_z) polarization is measured within in our experimental resolution. This is consistent with our calculations, where also zero out-of-plane spin polarization is found everywhere in the surface BZ. The lack of out-of-plane spin polarization is in fact guaranteed by symmetries, namely, time reversal symmetry $\mathcal{T}$ and two-fold rotational symmetry along the $\hat{z}$ axis C_{2z}. Specifically, in the surface BZ, the combined transformation $C_{2z}\mathcal{T}$ is a symmetry of every surface wavevector, i.e., it maps (k_x, k_y) to itself. Since $(\mathcal{T}C_{2z})^2 = +1$, this symmetry does not result in Kramers degeneracy, but rather $(\mathcal{T}C_{2z})|\psi(k_x, k_y)\rangle$ and $|\psi(k_x, k_y)\rangle$ are proportional up to a phase factor. Given further that $\mathcal{T}$ flips all spin components but C_{2z} only flips S_x and S_y, we obtain that the expectation value of S_z vanishes.

We also study the origin of the observed large spin polarization. We check the magnitude of the spin polarization in theoretical calculations. As shown in Fig. 4(b), the two bands that form a Kramers pair near the Fermi level at the $\bar{\Gamma}$ point are the two crescent Fermi arcs. The results in Fig. 4(b) show that the two Fermi arcs have opposite spin polarization direction and a polarization magnitude of about 85%. These results are consistent with the

experimental data (Figs. 2 and 3). To understand the large polarization, we decompose the total spin texture into contributions from different orbitals. In a spin-orbit coupled system, the physical spin is not a good quantum number as the eigenstates of the Hamiltonian are linear combinations of different orbitals and spins. In the case of TaAs, our calculation shows that the Fermi arcs arise from the As p_x orbital and the Ta d_{xz} and $d_{x^2-y^2}$orbitals. The spin textures of these orbitals sum up in a constructive way. Therefore, the total spin polarization is close to 100%. On the other hand, it is well known that the total spin polarization of Bi_2Se_3 surface states is only about 40% [36]. This is because the spin textures of p_x, p_y, and p_z orbitals add up destructively. It was proposed that one can using different light polarizations to selectively probe the spin polarization that arises from certain orbitals of the Bi_2Se_3 surface state [37]. References [38, 39] emphasized the role of the final state effect in laser-SARPES measurements on Bi_2Se_3, which means that electron-photon interactions can completely alter the spin orientation of the photoemission electrons relative to that of the Bi_2Se_3 surface states. In the presence of strong final state effects [38, 39], it is difficult to obtain information about the total Bi_2Se_3 spin texture from the laser-SARPES measurements. Reference [40] checked the final state effects in Bi_2Se_3 and the results showed that the laser-SARPES data were either consistent with the spin polarization of the surface states or with the final state effects depending on the experimental conditions including the incident photon energy, light polarization, etc. In the case of TaAs, all these have not been studied systematically yet. Our systematic data show that the spin measurements at 7 eV are consistent with the total spin polarization of the Fermi arcs. This demonstrates the value of our work in revealing the spin polarization of the Fermi arcs.

Finally, we investigate the topological "information" of the Fermi arc. We first briefly review the topological information that can be deduced without spin. As elaborated in Refs. [12, 18, 19], one can prove the Fermi arc nature of the surface states by resolving the sign of the Fermi velocity of the surface bands (Figs. 4(f,g)) along a k space loop that encloses a +2 projected Weyl node. As for the spin texture, the non-degenerate (spin polarized) property is important. If the surface bands were doubly degenerate, the chiral modes in Fig. 4(g) would give rise to a Chern number of +4, which is inconsistent with the chiral charge of +2 in the bulk. However, the non-degenerate property represents only a small fraction of the information from the Fermi arc spin texture. An obvious question to ask is that whether the texture, i.e., the k space configuration of the spin polarization, also carries

any topological meaning. One proposal is that one can infer the chirality of bulk Weyl cone by studying the spin texture of the Fermi arcs at the k points where the Fermi arcs and the bulk band projections merge with each other. However, we note that this proposal is not feasible in TaAs for the following reasons. First, a significant part of the bulk band projection arises from other irrelevant (non-Weyl) bulk Fermi surfaces (Fig. 4(d)). Second, the spin polarization of the Fermi arc does not match with that of the projected bulk bands at k points where they merge (Fig. 4(e)). We expect surface resonance states at k points where surface states enter the bulk. Hence the surface spin should slowly evolve and only become fully consistent with the bulk when it goes deeply into the bulk projection as the wavefunction become completely delocalized from the surface. Third, as can be seen from the red arrows in Fig. 4(e), the bulk spin texture does not follow the monopole/antimonopole configuration. In fact, the Weyl nodes are monopoles of Berry curvature, and the Berry curvature is in general different from the physical spin in a spin-orbit coupled system. Hence even if one were able to infer the bulk spin texture from the surface spin texture, it cannot prove the monopole property in the case of TaAs.

After the completion of this work, we became aware of the preprint [41]. We compare our data with the data reported in Ref. [41]. First, we observe a nearly full (80%) spin polarization as a consequence of the distinct orbital properties of TaAs Fermi arcs. Second, our data, in agreement with our calculations, show no observable out-of-plane spin polarization (P_z) at all k points studied. These observations are consistent with the calculated spin polarization of the Fermi arcs. Finally, our systematic calculations and data show that the spin texture of the Fermi arc cannot be used to infer the chirality of the Weyl nodes.

In summary, our observation provides a new type of spin texture that arises from a new type of 2D electron gas, the Fermi arc surface states. The spin texture is completely in-plane. The nearly full spin polarization is favorable for spin applications based on the Fermi arcs of TaAs.

[1] H. Weyl, I. Z. Phys. **56**, 330 (1929).

[2] C. Herring, Phys. Rev. **52**, 365 (1937).

[3] A. A. Abrikosov and S. D. Beneslavskii, J. Low T. Phys. **5**, 141 (1971).

[4] H. B. Nielsen and M. Ninomiya, Phys. Lett. B, **130**, 389 (1983).

[5] G. E. Volovik, *The Universe in a Helium Droplet* (Clarendon Press, Oxford, 2003).

[6] S. Murakami, New J. Phys. **9**, 356 (2007).

[7] X. Wan, A. M. Turner, A. Vishwanath, and S. Y. Savrasov, Phys. Rev. B **83**, 205101 (2011).

[8] A. A. Burkov and L. Balents, Phys. Rev. Lett. **107**, 127205 (2011).

[9] S.-Y. Xu, C. Liu1, S. K. Kushwaha, R. Sankar, J. W. Krizan, I. Belopolski, M. Neupane, G. Bian, N. Alidoust, T.-R. Chang, H.-T. Jeng, C.-Y. Huang, W.-F. Tsai, H. Lin, P. P. Shibayev, F.-C. Chou, R. J. Cava, and M. Z. Hasan, Science **347**, 294 (2015).

[10] S.-M. Huang, S.-Y. Xu, I. Belopolski, C.-C. Lee, G. Chang, B. Wang, N. Alidoust, G. Bian, M. Neupane, C. Zhang, S. Jia, A. bansil. H. Lin, and M. Z. Hasan, Nature Commun. **6**, 7373 (2015).

[11] H. Weng, C. Fang, Z. Fang, A. Bernevig, and X. Dai, Phys. Rev. X **5**, 011029 (2015).

[12] S.-Y. Xu, I. Belopolski, N. Alidoust, M. Neupane, G. Bian, C. Zhang, R. Sankar, G. Chang, Z. Yuan, C.-C. Lee, S.-M. Huang, H. Zheng, J. Ma, D. S. Sanchez, B. Wang, A. Bansil, F. Chou, P. P. Shibayev, H. Lin, S. Jia, and M. Z. Hasan, Science **349**, 613 (2015).

[13] L. Lu, Z. Wang, D. Ye, L. Ran, L. Fu, J. D. Joannopoulos, and M. Soljačić, Science **349** 622 (2015).

[14] C. Zhang, Z. Yuan, S.-Y. Xu, Z. Lin, B. Tong, M. Z. Hasan, J. Wang, C. Zhang, and S. Jia, arxiv:1502.00251 (2015).

[15] B. Q. Lv, H. M. Weng, B. B. Fu, X. P. Wang, H. Miao, J. Ma, P. Richard, X. C. Huang, L. X. Zhao, G. F. Chen, Z. Fang, X. Dai, T, Qian, and H. Ding, Phys. Rev. X **5**, 031013 (2015).

[16] B. Q. Lv, N. Xu, H. M. Weng, J. Z. Ma, P. Richard, X. C. Huang, L. X. Zhao, G. F. Chen, C. E. Matt, F. Bisti, V. N. Strocov, J. Mesot, Z. Fang, X. Dai, T. Qian, M. Shi, and H. Ding, Nature Phys. **11**, 724 (2015).

[17] S.-Y. Xu, N. Alidoust, I. Belopolski, Z. Yuan, G. Bian, T.-R. Chang, H. Zheng, V. N. Strocov, D. S. Sanchez, G. Chang, C. Zhang, D. Mou, Y. Wu, L. Huang, C.-C. Lee, S.-M. Huang, B. Wang, A. Bansil, H.-T. Jeng, T. Neupert, A. Kaminski, H. Lin, S. Jia, and M. Z. Hasan, Nature Phys. **11**, 748 (2015).

[18] S.-Y. Xu, I. Belopolski, D. S. Sanchez, C. Guo, G. Chang, C. Zhang, G. Bian, Z. Yuan, H. Lu, Y. Feng, T.-R. Chang, P. P. Shibayev, M. L. Prokopovych, N. Alidoust, H. Zheng, C.-C. Lee, S.-M. Huang, R. Sankar, F. Chou, C.-H. Hsu, H.-T. Jeng, A. Bansil, T. Neupert, V. N.

Strocov, H. Lin, S. Jia, and M. Z. Hasan, Science Advances **1**, e1501092 (2015).

[19] I. Belopolski, S.-Y. Xu, D. Sanchez, G. Chang, C. Guo, M. Neupane, H. Zheng, C.-C. Lee, S.-M. Huang, G. Bian, N. Alidoust, T.-R. Chang, B. Wang, X. Zhang, A. Bansil, H.-T. Jeng, H. Lin, S. Jia, and M. Z. Hasan, arxiv:1509.07465 (2015).

[20] H. Zheng, S.-Y. Xu, G. Bian, C. Guo, G. Chang, D. S.Sanchez, I. Belopolski, C.-C. Lee, S.-M. Huang, X. Zhang, R. Sankar, N. Alidoust, T.-R. Chang, F. Wu, T. Neupert, F.Chou, H.-T. Jeng, N. Yao, A. Bansil, S. Jia, H. Lin, and M. Z. Hasan, ACS Nano 10.1021/acsnano.5b06807 (2012).

[21] P. Hosur, Friedel oscillations due to Fermi arcs in Weyl semimetals. Phys. Rev. B **86**, 195102 (2012).

[22] H. Wei, S.-P. Chao, and V. Aji, Phys. Rev. Lett. **109**, 196403 (2012).

[23] P. Goswami and S. Tewari, Phys. Rev. B **88**, 245107 (2013).

[24] T. Ojanen, Phys. Rev. B **87**, 245112 (2013).

[25] Z. Wang and S.-C. Zhang, Phys. Rev. B **87**, 161107(R) (2013).

[26] A. C. Potter, I. Kimchi, and A. Vishwanath, Nature Commun. **5**, 5161 (2014).

[27] P. Hosur and X.-L. Qi, Phys. Rev. B. **90**, 045130 (2014).

[28] C.-K. Chan, P. A. Lee, K. S. Burch, J. H. Han, and Y. Ran, arxiv:1509.05400 (2015).

[29] T. Morimoto and N. Nagaosa, arxiv:1508.03203 (2015).

[30] M. Z. Hasan and C. L. Kane, Rev. Mod. Phys. **82**, 3045 (2010).

[31] D. Hsieh, Y. Xia, L. Wray, D. Qian, A. Pal, J. H. Dil, J. Osterwalder, F. Meier, G. Bihlmayer, C. L. Kane, Y. S. Hor, R. J. Cava, and M. Z. Hasan, Science **323**, 919 (2009).

[32] D. Hsieh, Y. Xia, D. Qian, L. Wray, J. H. Dil, F. Meier, J. Osterwalder, L. Patthey, J. G. Checkelsky, N. P. Ong, A. V. Fedorov, H. Lin, A. Bansil, D. Grauer, Y. S. Hor, R. J. Cava, and M. Z. Hasan, Nature **460**, 1101 (2009).

[33] J. P. Perdew, K. Burke, and M. Ernzerhof, Phys. Rev. Lett. **77**, 3865 (1996).

[34] J. J. Murray, J. B. Taylor, L. D. Calvert, Y. Wang, E. J. Gabe, and J. G. Despault, J. Less Common Met. **46**, 311 (1976).

[35] H. Weng, T. Ozaki, and K. Terakura, Phys. Rev. B **79**, 235118 (2009).

[36] O. V. Yazyev, J. E. Moore, and S. G. Louie, Phys. Rev. Lett. **105**, 266806 (2010).

[37] Y. Cao, J. A. Waugh, N. C. Plumb, T. J. Reber, S. Parham, G. Landolt, Z. Xu, A. Yang, J. Schneeloch, G. Gu, J. H. Dil, and D. S. Dessau, arXiv:1211.5998 (2012).

[38] C.-H. Park and S. G. Louie, Phys. Rev. Lett. **109**, 097601 (2012).

[39] C. Jozwiak, C.-H. Park, K. Gotlieb, C. Hwang, D.-H. Lee, S. G. Louie, J. D. Denlinger, C. R. Rotundu, R. J. Birgeneau, Z. Hussain, and A. Lanzara, Nature Phys. **9**, 293 (2013).

[40] J. Sánchez-Barriga, A. Varykhalov, J. Braun, S.-Y. Xu, N. Alidoust, O. Kornilov, J. Minr, K. Hummer, G. Springholz, G. Bauer, R. Schumann, L.?V. Yashina, H. Ebert, M.?Z. Hasan, and O. Rader, Phys. Rev. X **4**, 011046 (2014).

[41] B. Q. Lv, S. Muff, T. Qian, Z. D. Song, S. M. Nie, N. Xu, P. Richard, C. E. Matt, N. C. Plumb, L. X. Zhao, G. F. Chen, Z. Fang, X. Dai, J. H. Dil, J. Mesot, M. Shi, H. M. Weng, and H. Ding, Phys. Rev. Lett. **115**, 217601 (2012).

Acknowledgements: Work at Princeton University were supported by the Gordon and Betty Moore Foundations Emergent Phenomena in Quantum Systems Initiative through Grant GBMF4547 (Hasan). The work at the University of Tokyo was supported by Photon and Quantum Basic Research Coordinated Development Program from MEXT, and by JSPS Grant-in-Aid for Scientific Research (B), Grant No. 26287061 and for Young Scientists (B), Grant No. 24740197. Single-crystal growth was supported by the National Basic Research Program of China (grant nos. 2013CB921901 and 2014CB239302), and the sample characterization was supported by the U.S. Department of Energy (DOE), Office of Science, Basic Energy Sciences (BES) under the grant number DE-FG-02-05ER46200. Works at the National University of Singapore were supported by the National Research Foundation (NRF), Prime Ministers Office, Singapore, under its NRF fellowship (NRF award no. NRF-NRFF2013-03). T.-R.C. and H.-T.J. were supported by the National Science Council, Taiwan. H.-T.J. also thanks the National Center for High-Performance Computing, Computer and Information Network Center National Taiwan University, and National Center for Theoretical Sciences, Taiwan, for technical support. The work at Northeastern University was supported by the by the DOE/BES under the grant number DE-FG02-07ER46352, and benefited from Northeastern Universitys Advanced Scientific Computation Center (ASCC) and the NERSC supercomputing center through DOE grant number DE-AC02-05CH11231. We gratefully thank A. Alexandradinata for helpful discussions. M.N. was supported by the start-up funds from University of Central Florida and the Los Alamos National Laboratory through the Laboratory Directed Research & Development program. S.M.H., G.C., T.R.C,

and H.L.'s visits to Princeton University were partially funded by the GBMF4547 (Hasan).

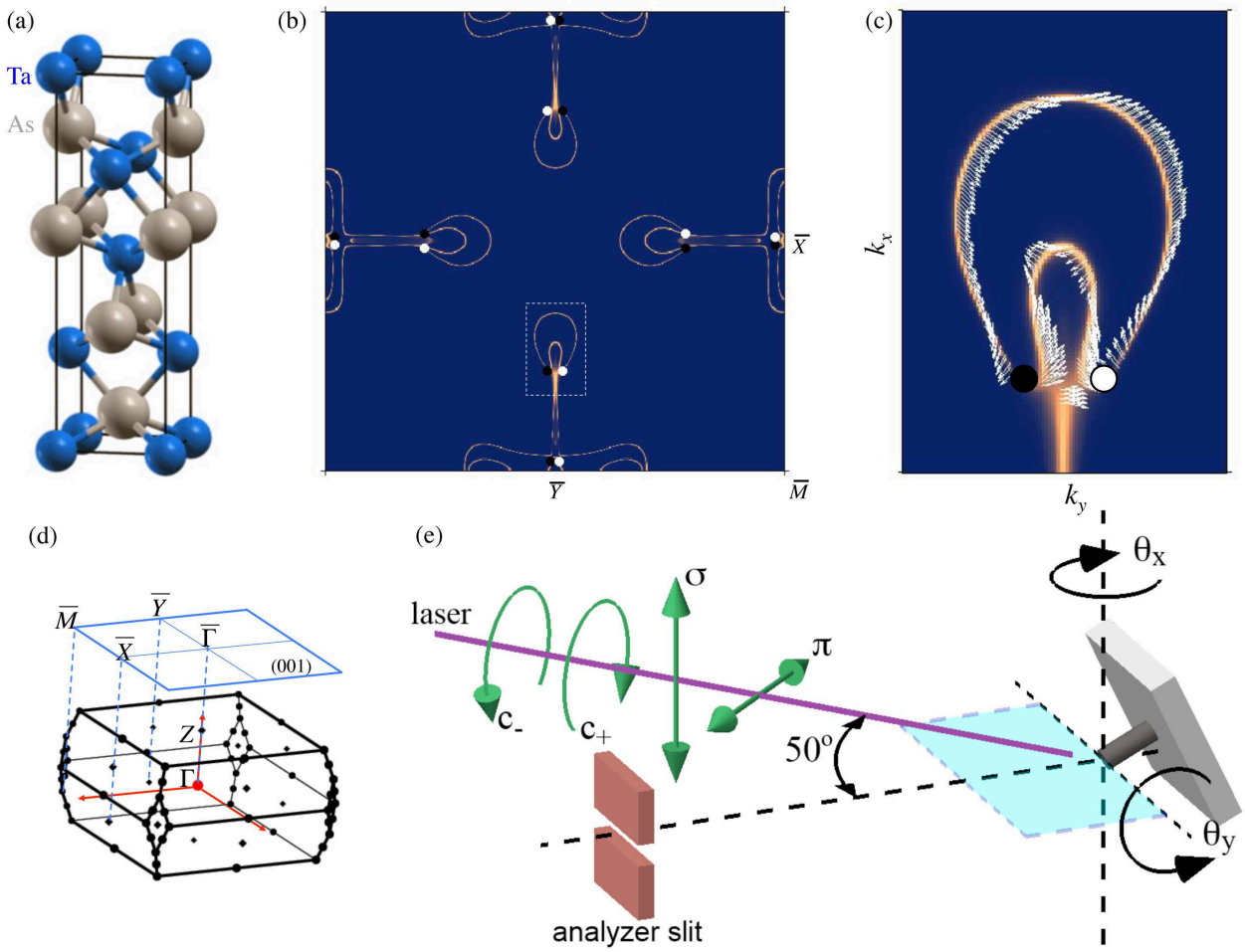

FIG. 1: **Theoretically calculated surface band structure and spin texture.** (a) Body-centered tetragonal structure of TaAs, shown as stacks of Ta (blue) and As (silver) layers. The screw-like pattern along the z-direction leads to a non-symmporphic C_4 rotation symmetry that includes a translation along the z-direction by $c/4$. The lattice of TaAs lacks space inversion symmetry. (b) First-principles band structure calculation of the (001) surfaces states of TaAs. The black and white circles indicate the projected Weyl nodes with opposite chirality. (c) Corresponding theoretical spin texture of Fermi arc surface states. The k-space range is defined by the white dotted box in (b). (d) The bulk and (001) surface Brillouin zone of TaAs. High symmetry points are noted. (e) Experimental geometry of the spin-resolved ARPES instrument.

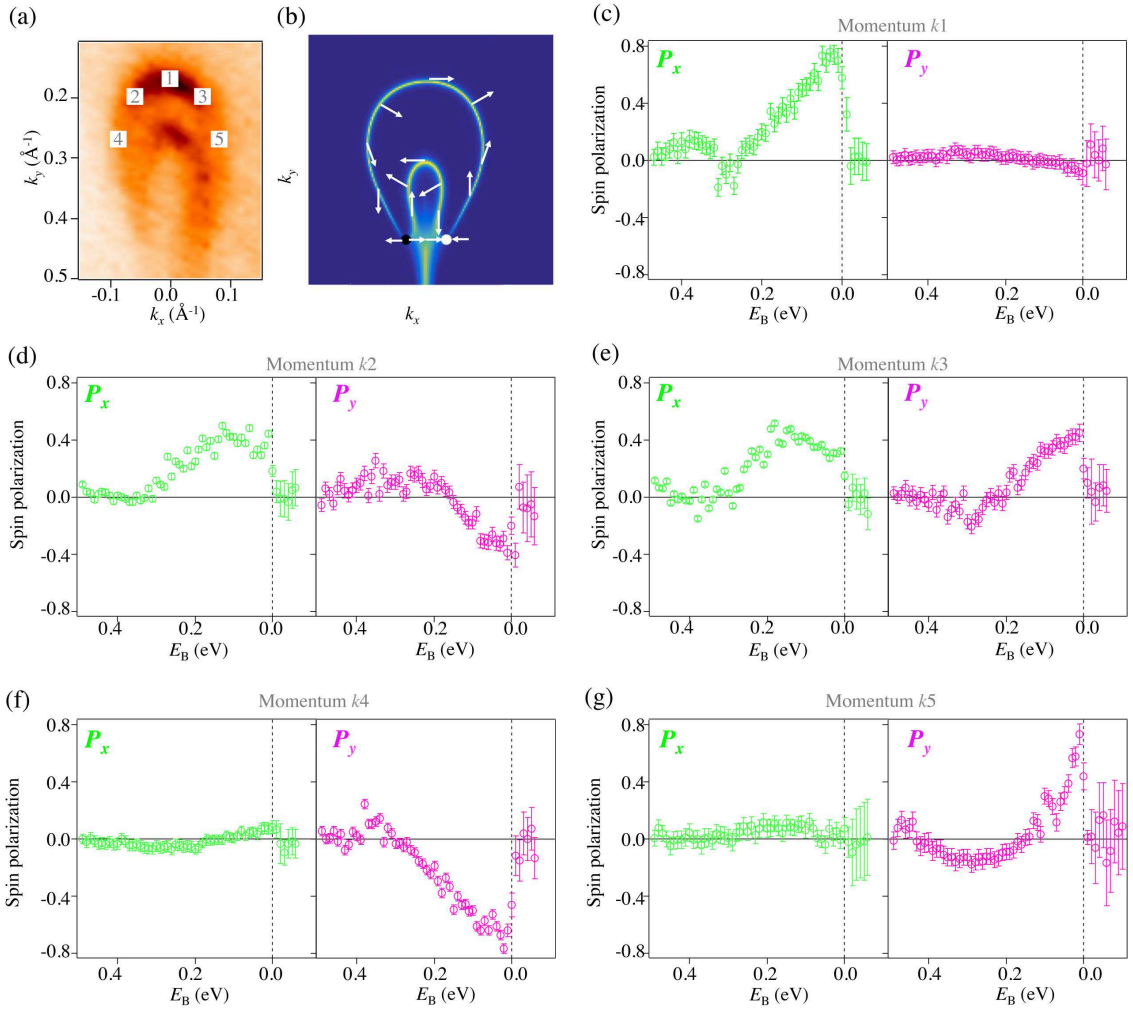

FIG. 2: **Spin texture measurement of outer Fermi arc.** (a) High-resolution ARPES Fermi surface map of crescent Fermi arcs measured with incident photon energy of 90 eV. Numbers 1, 2, 3, 4, and 5 indicate the k locations where spin-resolved ARPES measurements were performed on the outer arc. (b) Schematic illustration of the spin texture. The arrows show the direction of spin polarization on selective k points on the Fermi arcs based on our calculations. (c-g) Measured in-plane spin polarization at 1-5 correspond to panels denoted by k_1, k_2, k_3, k_4, and k_5, respectively.

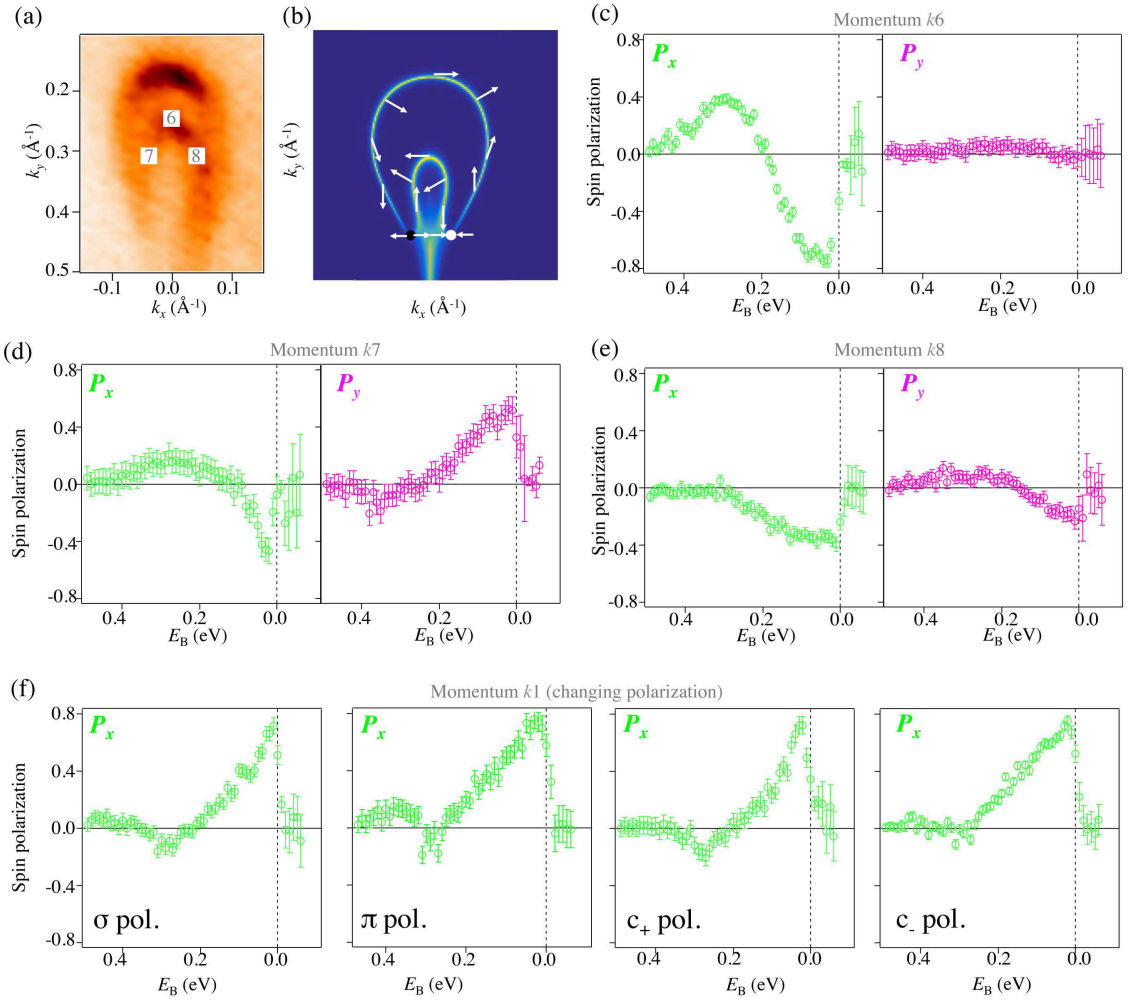

FIG. 3: **Spin texture measurement of inner Fermi arc.** (a) High-resolution ARPES Fermi surface map of crescent Fermi arcs. Numbers 6, 7, and 8 indicate the k locations where spin-resolved ARPES measurements were performed on the inner arc. (b) Schematic illustration of the spin texture. The arrows show the direction of spin polarization on selective k points on the Fermi arcs based on our calculations. (c-g) Measured in-plane spin polarization at 6-8 correspond to panels denoted by k_6, k_7, and k_8, respectively. (f) Spin polarization measurements at k_1 using different polarizations of the incident light polarization.

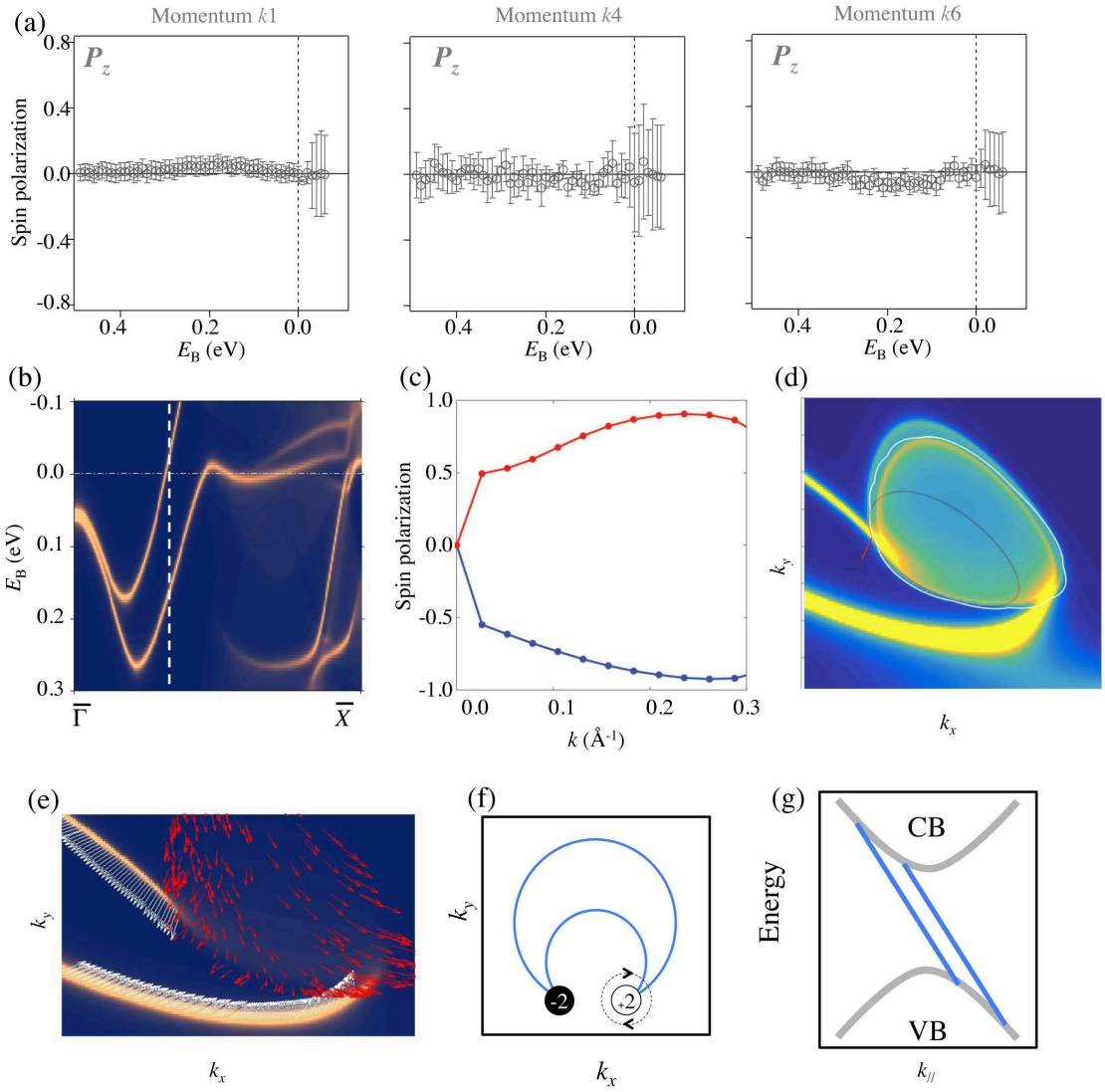

FIG. 4: **Lack of out-of-plane spin polarization, large spin polarization magnitude, and deviation between spin textures of the Fermi arc and Weyl cones.** (a) Spin polarization measurements along the out-of-plane direction for k_1, k_4, and k_6. No out-of plane spin polarization is measured within in our experimental resolution. (b) Theoretically calculated surface energy dispersion along $\bar{\Gamma} - \bar{X}$. (c) The magnitude of spin polarization for the two bands that form a Kramers' pair near the Fermi level at the $\bar{\Gamma}$ point in panel (b). These two bands arise from the two Fermi arcs of one crescent-shaped feature. The range of the x axis is from the $\bar{\Gamma}$ point to the white dotted lines in panel (b).(d) A zoomed-in calculation near a projected Weyl node slightly above the Fermi level. The two Fermi arcs are seen to merge into the bulk band projection, which is noted by the white contour.

FIG. 4: The black contour shows the projection of the Weyl cones only. We see that the total projection (white contour) is larger than the Weyl cone projection (black contour). This demonstrates that there are additional irrelevant (non-Weyl) bulk Fermi surfaces contributing to the bulk projection. (e) The spin-texture calculation for (d), which shows the spin-polarization of the Fermi arc surface states with white arrows, and red arrows for the bulk pocket around the Weyl node. (f) A schematic showing crescent shaped Fermi arcs (blue curve) connecting to projected Weyl nodes. (g) An illustration of the band structure along the black dotted circle.